Design and performance evaluation of a high temperature axisymmetric plug nozzle

Ahmed ABDALLAH ELHIRTSI*,[1], Toufik ZEBBICHE[1]

*Corresponding author

[1]Aeronautical Sciences Laboratory, Aeronautics and Space Studies Institute,
Blida 1 University, BP 270 Blida 09000, Algeria,
abdallah.elhirtsi.a@gmail.com*

Abstract: *In this study, a method for designing supersonic nozzles with axisymmetric plugs at high temperature has been proposed. The approach is based on the theory of Prandtl-Mayer expansion at high temperatures using the method of characteristics. For this purpose, a code in FORTRAN language was developed in order to obtain the nozzle design. Once the latter was obtained, we were interested in the evolution of the thermodynamic parameters of the flow such as pressure, temperature, and Mach number. The results achieved were confronted with those obtained for a perfect gas model. Regarding the design parameters (length, section ratio, thrust coefficient and mass coefficient), we found that the PG model gives very satisfactory results for values of M and T_0 below 2.00 and 1000 K, respectively. As M_E and T_0 increase, this affects performance, requiring the use of our HT model to correct the calculations. In order to minimize the weight of this nozzle, this research is investigating the truncation of the Plug nozzle to increase its performances. All calculations were performed for air.*

Key Words: *Supersonic axisymmetric nozzle design, Plug nozzle, Prandtl-Meyer function, High temperature, Method of characteristics*

1. INTRODUCTION

In this work, we will focus on the study of the plug nozzle. This is an advanced rocket nozzle that consists of a primary nozzle of a rather conventional shape and a plug that allows external expansion. The main characteristics of this nozzle are its interaction with the external environment, which avoids the separation phenomenon that affects a conventional profile nozzle, and its influence on the pressure evolution along the plug wall [1]. The plug nozzle concept was first developed by the Germans before World War II for aeronautical applications. Rolls-Royce, Ltd proposed the plug nozzle concept for rocket propulsion in the United States in 1950 [2]. Plug nozzles have a central body near the throat and the gas expansion process is directly or indirectly regulated by the ambient pressure, the gas flow is regulated by expansion waves from the flow deflection due to the surface of the plug [3]. The plug nozzle rocket engine is considered as a better alternative for space propulsion, compared to conventional nozzles [4]. Many researchers have been interested in the study of these nozzles. These studies have focused on contour design [5, 3, 6], performance and parameters of the flow field [7, 8]. Among these studies, there are experimental studies [9] and experimental numerical studies [10, 11, 12]. All these works considered that the gas is perfect and assumed that the specific

heat C_P is a constant value that does not vary with temperature. For values of $M_E = 2$ and $T_0 = 240\,K$, the results obtained are very satisfactory. For values of the output Mach number ranging from 2 to 5, and the temperature increases up to the limit value of $3550K$ (air application), which is the case for most aerospace applications, the results diverge from reality, because the physical behavior of the gas changes, and it becomes calorically imperfect and thermally perfect. In this case, the specific heat C_P becomes a function of temperature and the energy conservation equation changes completely [13]. The appropriate model in this case is the High Temperature (HT) model, which is below the dissociation threshold of the molecules. It depends mainly on the stagnation temperature, which becomes an important parameter, in addition to the parameters of the Perfect Gas (PG) model [13].

The objective of this work is to achieve two goals, the first of which is to determine a new shape of axisymmetric supersonic plug nozzle (PN) giving a uniform and parallel flow at the exit section at high temperature, in order to make corrections to the results given by the Perfect Gas model [14, 15]. The second objective will be dedicated to the determination of the parameters (Flow angle deviation at Critical condition θ^*, Length of the plug nozzle/ Polar radius at exit section $\dfrac{L}{\lambda_E}$, Exit section/Throat section $\dfrac{A_E}{A^*}$, Static pressure/Total pressure $\dfrac{P}{P_0}$, Static temperature/Total temperature $\dfrac{T}{T_0}$ and Density $\dfrac{\rho}{\rho_0}$) in the flow field points for the axisymmetric plug nozzle.

2. MATHEMATICAL FORMULATION

Fig. 1 below shows the flow field in a 2D Plug Nozzle (Fig. 1a) and the Expansion Deflexion Nozzle (EDN) (Fig. 1b). The PN has a central body and the EDN has an external wall which must be determined to have a uniform flow parallel to the exit section. The design method is an accurate method based on the Prandtl-Meyer expansion.

The plug nozzle is characterized by an inclination of an angle θ^* with regard to the horizontal, as seen in Fig. 2. This is different from other designs where the flow is horizontal at the throat.

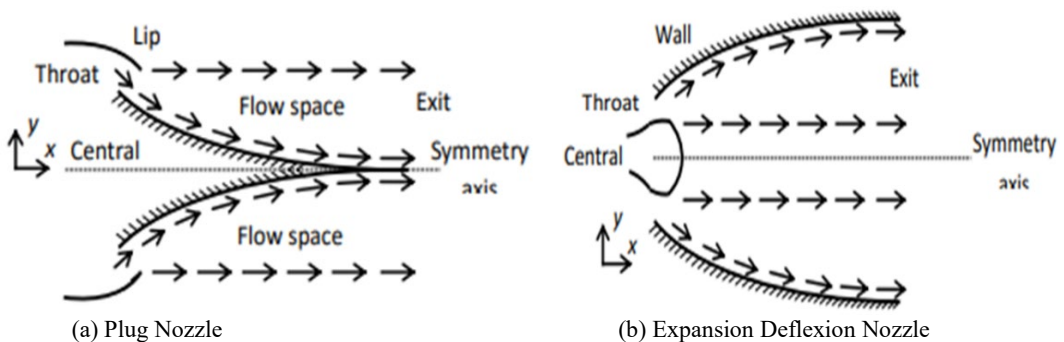(a) Plug Nozzle   (b) Expansion Deflexion Nozzle

Fig. 1 – Type of plug nozzle geometry

The lip of the central body must be inclined at an angle Ψ to the vertical. Because the flow deviation at the throat is not zero, the flow straightens from the angle $\theta = \theta^*$ at the throat to the angle $\theta = 0$ at the exit. The flow must thus be accelerated by the nozzle shape from the throat, where the Mach number is $M^* = 1$, to the exit section, where the Mach number is ME. This configuration results in a parallel and uniform flow in the exit area of the nozzle. The expansion of the axisymmetric plug nozzle generates only an ABE transition area, which represents a non-simple wave region for which a numerical solution is achieved [16].

However, the zone AES is a uniform flow zone with an exit Mach number M_E (see Fig. 2 and Fig. 3).
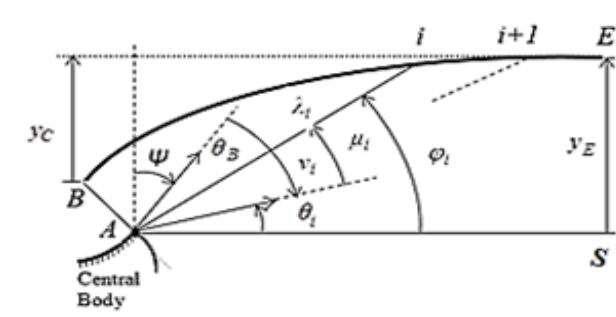

Fig. 2 – Geometry relationship between Mach lines and flow direction

Based on the Prandtl-Meyer expansion [13, 16], the flow calculation and the contour of the HT plug nozzle are determined by

$$\theta_E = v_E = \int_{T_E}^{T^*} F_V(T) \, dT \tag{1}$$

with:

$$F_V(T) = -\frac{C_P(T)}{2H(T)} \sqrt{\frac{2H(T)}{a^2(T)} - 1} \tag{2}$$

and

$$a(T) = \sqrt{\gamma(T)RT}; \, M(T) = \sqrt{2M(T)} \tag{3}$$

The relationship that determines the inclination of the lip in reference to the vertical is given by Eq. (4), [13, 16]. v_E represents the Prandtl-Meyer function.

$$\Psi = 90 - v_E \tag{4}$$

2.1 Discretization

The profile of the axisymmetric plug nozzle is determined simultaneously with the flow calculation at the point of intersection of the characteristics in the transition region ABE. The uniform flow values of the exit section M_E are identical to the known properties of the points on the control surface AE. The shape of the mesh in the transition area is controlled by the distance Δ_x specified for the selected points on the uniform Mach line AE. Figure 3 illustrates the calculating process and direction in the transition region.
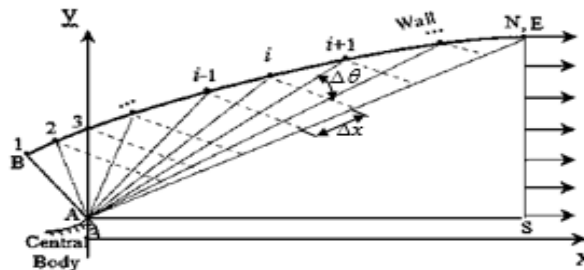

Fig. 3 – Process of the discretization of the plug nozzle

The following system gives the properties in positions A and B

Point A   Point B

$$
\begin{cases}
\begin{aligned}
x_A &= 0 \\
r_A &= 0 \\
\theta_i &= (i = 1)\frac{\theta^*}{N} \\
v_i &= \theta^* - \theta_i \\
M_i &= f(v_i) \\
\mu_i &= \sin^{-1}\left(\frac{1}{M_i}\right) \\
avec:& i = 1 \text{ à } (n+1)
\end{aligned}
\end{cases}
;
\begin{cases}
\begin{aligned}
x_b &= x_A - r_c \sin\phi \\
r_b &= r_A + r_c \cos\phi \\
\theta_B &= \theta^* \\
v_B &= 0 \\
M_B &= 1 \\
\mu_B &= \frac{\pi}{2}
\end{aligned}
\end{cases}
\tag{5}
$$

2.2 Calculation procedure

The implementation of the MOC (Method of Characteristics) requires the introduction of a fine grid in order to approximate each characteristic between two points by straight segments because C^- and C^+ are curved.

The characteristics of the following point (3) may be determined since a point in the supersonic flow field is associated to two characteristics, one ascending $C^+{}_{(1)}$ and the other descending $C^-{}_{(2)}$. The point (2) of the control surface A_E is determined by the properties given by Eq. (6).

$$
\begin{cases}
\begin{aligned}
x_2 &= x_A + \Delta x \cos\mu_E \\
y_2 &= r_A + \Delta x \sin\mu_E \\
\theta_2 &= 0 \\
v_2 &= v_E \\
M_2 &= \sin^{-1}\left(\frac{1}{M_2}\right)
\end{aligned}
\end{cases}
\tag{6}
$$

As illustrated in Fig. 4, the first step is to calculate the first characteristic, C, and determine its corresponding location on the nozzle wall.
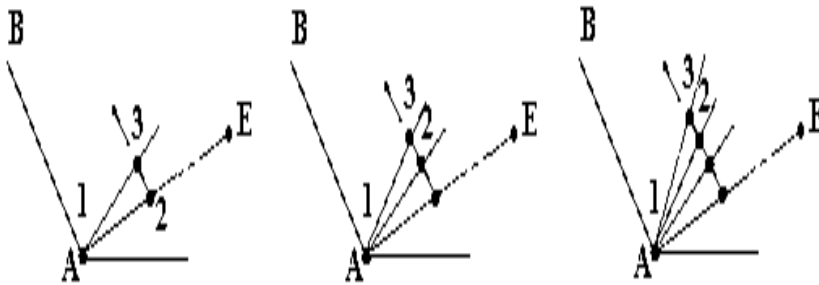

Fig. 4 – Calculation process of C^-

The iterative methodology is based on the mean of the position and original properties of the characteristics $C^-{}_{(2)}$ and $C^+{}_{(1)}$ as well as the location and mean of the position and properties of the point (3).

They will be utilized as initial conditions for their respective characteristics each time. This method is performed until the flow direction convergence conditions are satisfied (see Fig. 5).
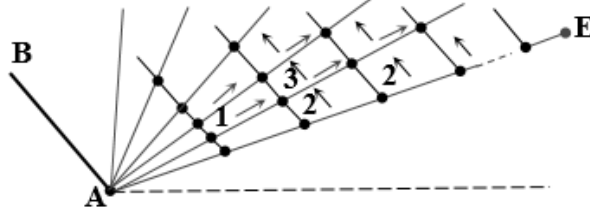
Fig. 5 – Determination of the different characteristics C^- and C^+

The MOC provides the following equations for the axisymmetric supersonic, non-rotational, adiabatic flow of a perfect gas, defined as characteristics and compatibilities equations [13, 15, 16, 17]:

1. Along C^-:

$$\begin{cases} d(\theta + v) = \dfrac{\sin\theta \sin\mu}{y\cos(\theta - \mu)} dy \\ \dfrac{dy}{dx} = \tan(\theta - \mu) \end{cases} \tag{7}$$

2. Along C^+:

$$\begin{cases} d(v - \theta) = \dfrac{\sin\theta \sin\mu}{y\cos(\theta - \mu)} dy \\ \dfrac{dy}{dx} = \tan(\theta + \mu) \end{cases} \tag{8}$$

Because the $H(T)$ function is impacted by the parameter T_0 [16], the HT model is primarily affected by the stagnation temperature T0 of the combustion chamber. The corresponding formulas to the HT model of the MOC are developed by modification of Eqs. (7) and (8) [16]:

Along C^+:

$$\begin{cases} \displaystyle\int_{T_{i-1}}^{T_{i+1}} \left[-\frac{C_P(T)}{2H(T)}\sqrt{M^2(T) - 1} \right] dT + \int_{\theta_{i-1}}^{\theta_{i+1}} d\theta = \int_{x_{i-1}}^{x_{i+1}} \frac{\sin\theta \sin\mu}{y\cos(\theta - \mu)} dx \\ \displaystyle\int_{T_{i-1}}^{T_{i+1}} dy = \int_{x_{i-1}}^{x_{i+1}} \tan(\theta - \mu)\, dx \end{cases} \tag{9}$$

1. Along C^+:

$$\begin{cases} \displaystyle\int_{T_{i-1}}^{T_{i+1}} \left[-\frac{C_P(T)}{2H(T)}\sqrt{M^2(T) - 1} \right] dT + \int_{\theta_{i-1}}^{\theta_{i+1}} d\theta = \int_{x_{i-1}}^{x_{i+1}} \frac{\sin\theta \sin\mu}{y\cos(\theta + \mu)} dx \\ \displaystyle\int_{T_{i-1}}^{T_{i+1}} dy = \int_{x_{i-1}}^{x_{i+1}} \tan(\theta + \mu)\, dx \end{cases} \tag{10}$$

It is important to use the proper approximations for evaluating the integrals in Eqs. (9) and (10), taking into consideration both the mathematical and physical properties of the interval. Characteristics and compatibilities equations are common non-linear equations. The application of the finite difference approach will be used to determine their solution [18]. The mesh created assumes the characteristic that is between two points joined by straight line segments. The predictor-corrector form of Euler's numerical integration approach is used [16, 19, 20]. The iterations of the Euler corrector algorithm are repeated until reaching the desired accuracy ε.

3. THE PERFECT GAS MODEL'S ERROR

A comparison of the results obtained by the two models will be conducted. The relative error for the PG model compared to the HT model for each design parameter can be calculated using the following relation for each value of the stagnation temperature T_0 and the exit Mach number M_E:

$$\varepsilon_{(Parameter)}\% = \left| \frac{(Parameter)_{HT} - (Parameter)_{GP}}{(Parameter)_{HT}} \right| 100 \tag{11}$$

Where $(Parameter)_{PG}$ and $(Parameter)_{HT}$ are, respectively, the values of the parameters that were estimated using the PG and the HT models.

4. RESULTS AND COMMENTS

The axisymmetric plug nozzle design results are presented in non-dimensional form for three stagnation temperatures $T_0 = 1000\ K$, $T_0 = 2000\ K$ and $T_0 = 3000\ K$. For each parameter, the ideal gas condition is given, with one application developed solely for air. The specific heat function C_P and the universal gas constant of the perfect gas R for the air case are applied in this application.

### 4.1 Grid in the characteristics

Figure 6 shows the grids in their characteristics by utilizing the many elements that have an impact on the development of the grid.

Each variable has a significance that determines the design final. The nature of a supersonic flow is determined by the conditions upstream. An initial calculation error (throat) progressed, being fairly significant in the exit section. In addition, the errors resulting from artificial viscosity in mathematical calculations. The chosen case assumes that $M_E = 3.00$ and $T_0 = 2000\ K$.

When the grid in the expansion zone between the throat and exit section's Mach waves is refined in Fig. 6, we can discretize this zone into N Mach waves (NC). Three examples are given for instances (a), (b), (c), and (d), using $NC = 10$, $NC = 30$, and $NC = 50$, respectively. It is observed that when the Mach waves number NC increases, we obtain an excellent representation of the main body. The refining in this region can then reduce the error. y* represent the throat radius.
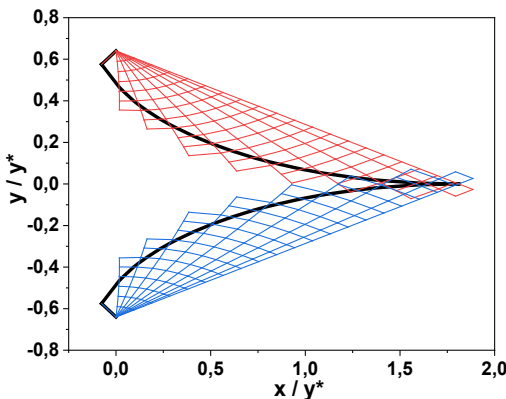
(a) $NC = 10$ and $\Delta_x = 0.1$ Large grid
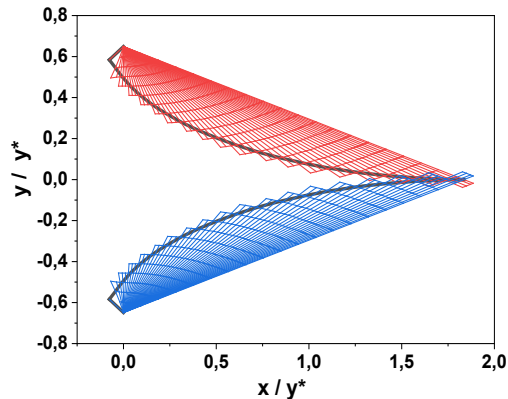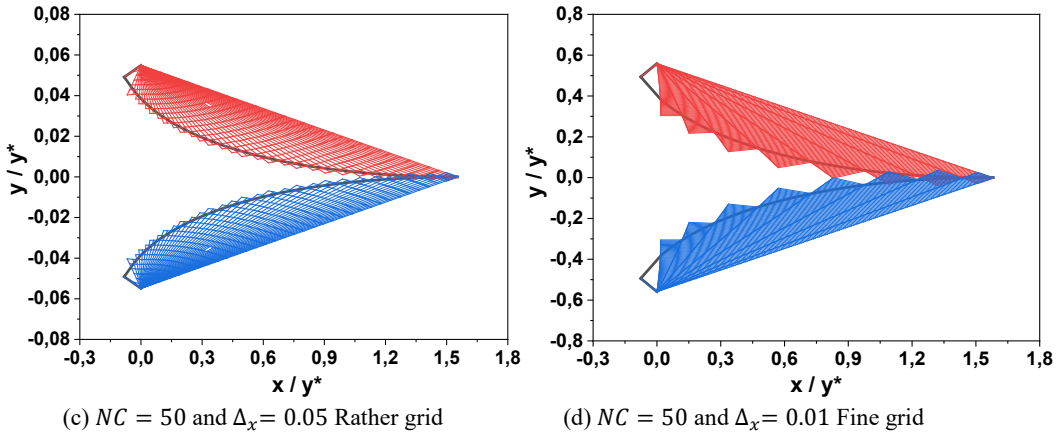

(b) $NC = 30$ and $\Delta_x = 0.1$ Moderate grid

(c) $NC = 50$ and $\Delta_x = 0.05$ Rather grid

(d) $NC = 50$ and $\Delta_x = 0.01$ Fine grid

Fig. 6 – Contour and mesh of nozzle for $M_E = 3.00$ and $T_0 = 2000\ K$

It is obvious that a greater number of points NC provides excellent presentation of the plug nozzle contour (Fig. 6d). The ratio of the sections is used to control the results, which is always correct because the flow at the nozzle exit is uniform and parallel. It should be noticed that design parameters depend on the pitch Δ_x and the volume of characteristics NC. The refining of the grid is due to better convergence and higher resolution.

Figures 7-10 show the temperature effect on the plug shape for different exit Mach number M_E ($M_E = 1.5, 2.00, 3.00$ and 4.00). C_m represents the coefficient of the mass of the structure.
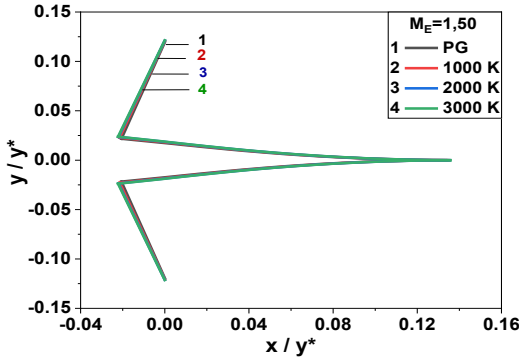

Fig. 7 – Temperature effect on the plug shape giving $M_E = 1.5$
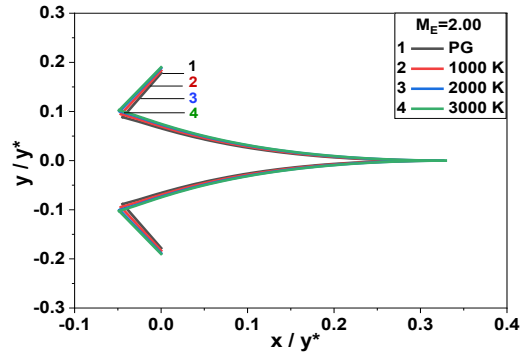

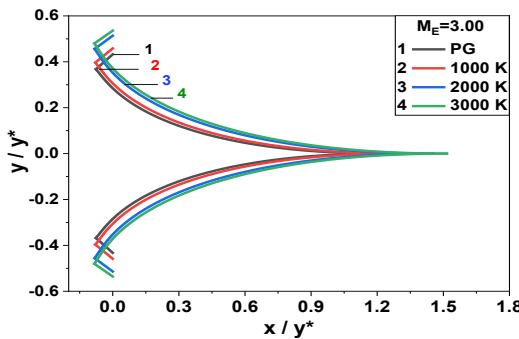Fig. 8 – Temperature effect on the plug shape giving $M_E = 2.00$

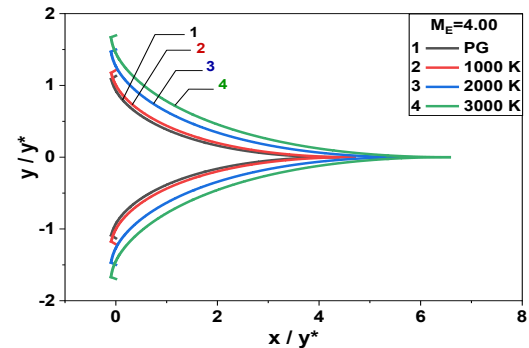Fig. 9 – Temperature effect on the plug shape giving $M_E = 3.00$

Fig. 10 – Temperature effect on the plug shape giving $M_E = 4.00$

Table 1 – Numerical results of Plug Shape for Fig. 7

$M_E = 1.50$	$\dfrac{L}{y^*}$	$\dfrac{A_S}{A^*}$	C_{mass}	C_F
PG	0.13365	1.17592	1.53604	0.09103
$T_0 = 1000\ K$	0.13472	1.18438	1.54739	0.09729
$T_0 = 2000\ K$	0.13539	1.18981	1.56881	0.10203
$T_0 = 3000\ K$	0.13563	1.19167	1.64006	0.12373

Table 2 – Numerical results of Plug Shape for Fig. 8

$M_E = 2.00$	$\dfrac{L}{y^*}$	$\dfrac{A_S}{A^*}$	C_{mass}	C_F
PG	1.22333	4.22003	13.49941	0.75008
$T_0 = 1000\ K$	1.29684	4.47133	14.30399	0.80023
$T_0 = 2000\ K$	1.45267	4.99581	15.97384	0.88816
$T_0 = 3000\ K$	1.51574	5.20999	18.23161	0.98652

Table 3 – Numerical results of Plug Shape for Fig. 9

$M_E = 3.00$	$\dfrac{L}{y^*}$	$\dfrac{A_S}{A^*}$	C_{mass}	C_F
PG	1.22333	4.22003	13.49941	0.75008
$T_0 = 1000\ K$	1.29684	4.47133	14.30399	0.80023
$T_0 = 2000\ K$	1.45267	4.99581	15.97384	0.88816
$T_0 = 3000\ K$	1.51574	5.20999	18.23161	0.98652

Table 4 – Numerical results of Plug Shape for Fig. 10

$M_E = 4.00$	$\dfrac{L}{y^*}$	$\dfrac{A_S}{A^*}$	C_{mass}	C_F
PG	4.37544	10.6470	43.46563	1.13114
$T_0 = 1000\ K$	4.69795	11.3912	46.35709	1.19075
$T_0 = 2000\ K$	5.80648	13.8615	58.73796	1.37478
$T_0 = 3000\ K$	6.57013	15.5141	65.02532	1.44654

The different design parameters (iso-Mach, pressure ratios $\frac{P}{P_0}$, temperature ratios $\frac{T}{T_0}$, and densities $\frac{\rho}{\rho_0}$) of the axisymmetric plug nozzle are shown in the contours of the flow fields obtained numerically by our calculation code and the numerical simulation (Fig. 11-14).

Figures 11b, 12b, 13b and 14b show the wall Mach number, wall pressure ratio, wall tempreature ratio and wall density comparison between the numerical method (FORTRAN code) and the simulation for $M_E = 3.00$ and $T_0 = 2000\ K$. The results show a good similarity.

The pressure ratio first falls rapidly at the nozzle throat expansion region until it reaches a value of 0.097432, then it continues to fall in the expansion part, and then it finally stabilizes at the tip of the nozzle, approaching the value of the atmospheric pressure at the tip of the nozzle at a value of 0.024394.

We note that in the divergent part, the number of Mach increases until reaching the value of the nozzle exit Mach number at the exit.

We notice that the number of Mach at the exit of the plug nozzle is $M = 3.0$. Figures 11a, 12a, 13a and 14a show the Iso-Mach, iso-pressure, iso-temerature and iso-density
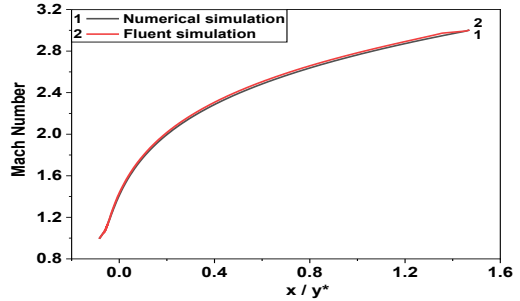
contours for a plug nozzle that works in the design Mach number obtained by our FORTRAN code.

It is visualized using Tecplot visualization software. It is noted that the flow increases from $M = 1$ in the throat until $M = design\ Mach$.
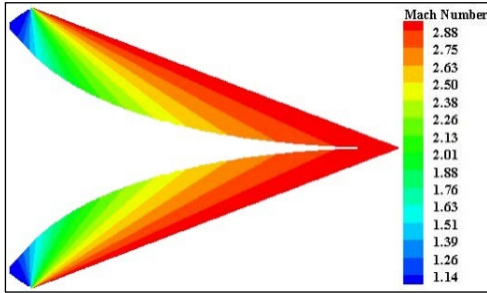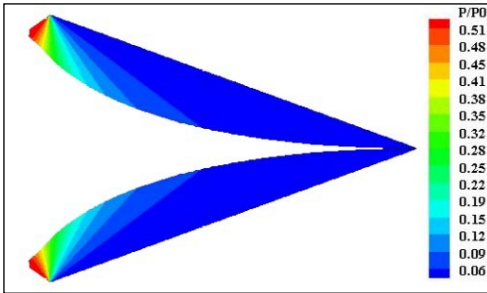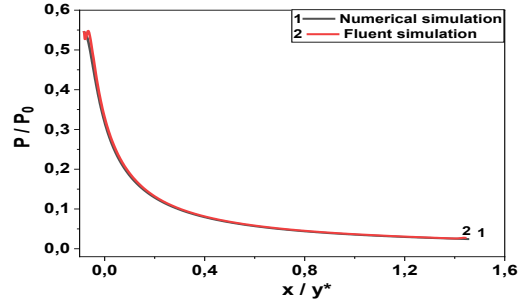

(a) Numerical results of the iso-Mach number curves

(b) Comparison results between the numerical and Fluent simulation

Fig. 11 – Variation of Mach number along the wall of the axisymmetric plug nozzle for $M_E = 3.00$ and $T_0 = 2000\ K$ with the results of the FORTRAN program
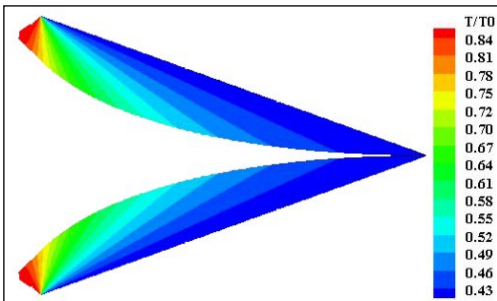

(a) Numerical results of the iso-Pressure $\frac{P}{P_0}$ curves
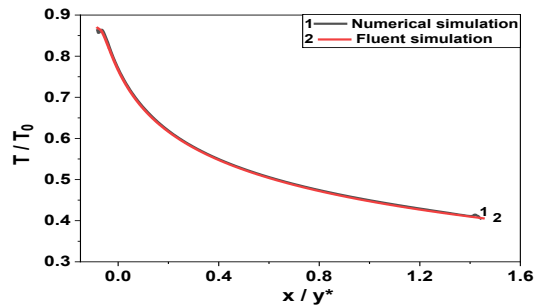
(b) Comparison results between the numerical and Fluent simulation

Fig. 12 – Variation of P/P_0 along the wall of the axisymmetric plug nozzle for $M_E = 3.00$ and $T_0 = 2000\ K$ with the results of the FORTRAN program
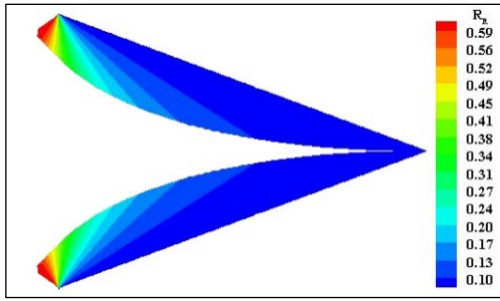

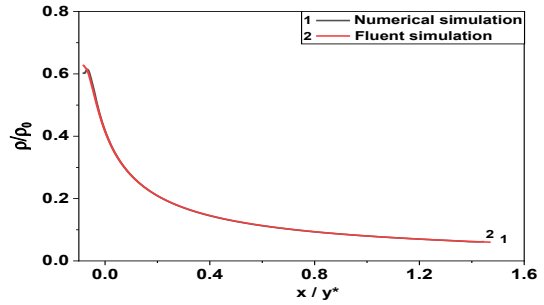(a) Numerical results of the iso-Temperature $\frac{T}{T_0}$ curves

(b) Comparison results between the numerical and Fluent simulation

Fig. 13 – Variation of T/T_0 along the wall of the axisymmetric plug nozzle for $M_E = 3.00$ and $T_0 = 2000\ K$ with the results of the FORTRAN program

(a) Numerical results of the iso-density $R_R = \frac{\rho}{\rho_0}$ curves

(b) Comparison results between the numerical and Fluent simulation

Fig. 14 – Variation of ρ/ρ_0 along the wall of the axisymmetric plug nozzle for $M_E = 3.00$ and $T_0 = 2000\,K$ with the results of the FORTRAN program

Figure 15 illustrates the variation of the flow deflection angle along the wall of the axisymmetric plug nozzle.

We note the existence of a point of inflection closer to the throat of the nozzle noted θ^* (where $M = 1$), then increases along the wall until reaching the maximum value θ_{max} at the point of deviation and decreases to $\theta_E = 0$ at the exit section where the flow is uniform and parallel (where $M = M_E$).

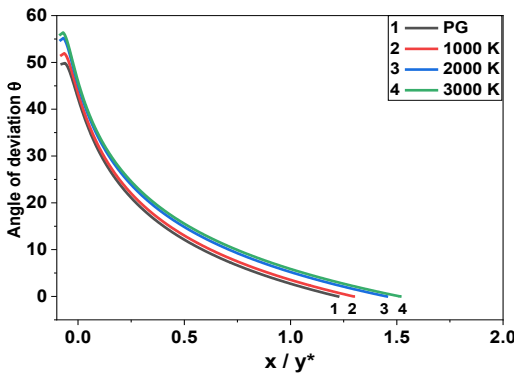In this case, the nozzle gives high efficiency and low losses.

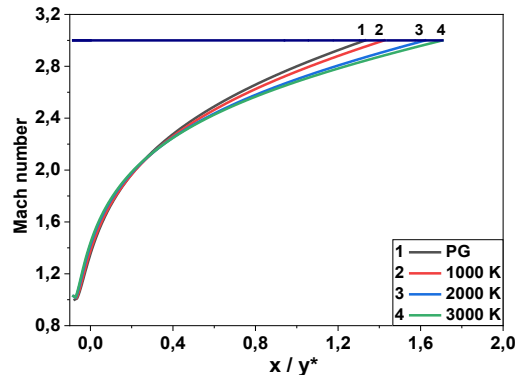Fig. 15 – Variation of the angle of deviation θ^* along the wall for $M_E = 3.00$

Fig. 16 – Variation of the Mach number along the wall of the plug nozzle for $M_E = 3.00$

Figure 16 shows the variation of the Mach number M along the wall of the axisymmetric plug nozzle for different values of the generating temperature T_0 as well as the case of an ideal gas, for an imposed exit Mach number $M_E = 3.00$.

We notice that the length difference between PG and HT Model is 6.43% for $T_0 = 1000K$. We also note that this percentage increases as T_0 increases until it reaches a percentage equal to 21.95% at $T_0 = 3000K$.

Figure 17 and 18 respectively illustrate the evolution of the temperature and pressure ratios along the contour of the axisymmetric plug nozzle for different values of the generating temperature T_0 for an imposed exit Mach number $M_E = 3.00$.

It can be seen that the temperature ratio is maximum at the throat. This ratio allows us to appropriately choose the constructive material resistant to this temperature.

The pressure ratio is used to determine the pressure force exerted on the nozzle wall. This ratio is also used to study the distribution of radial and tangential stresses in order to determine

the strength of the material. There is a sudden drop in pressure which will be completely transformed into thrust energy (to determine the thrust coefficient C_F).
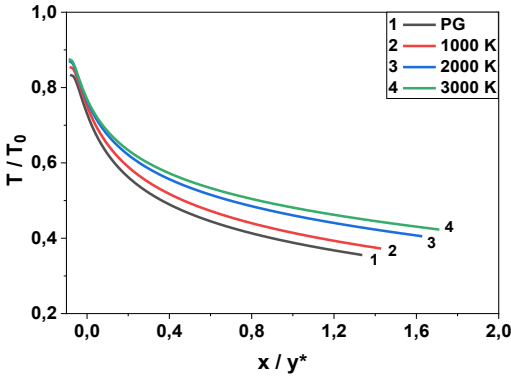

Fig. 17 – Variation of the temperature along the wall of the axisymmetric PN for $M_E = 3.00$
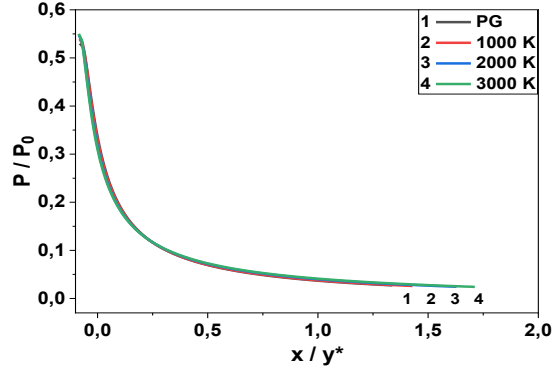
Fig. 18 – Variation of the pressure along the wall of the axisymmetric PN for $M_E = 3.00$

Figure 19 illustrates the variation of the length of the axisymmetric plug nozzle versus the exit Mach number M_E and the temperature T_0.

It is observed that the length of the plug nozzle increases not only with the increase in the exit Mach number M_E, but also with the increase in T_0.

It is concluded that more the nozzle delivers a higher exit Mach number, longer than the length of the plug nozzle becomes.

For T_0 equals $3000\ K$, there is a difference in the length of the plug nozzle between PG and HT model estimated at 18.41%.
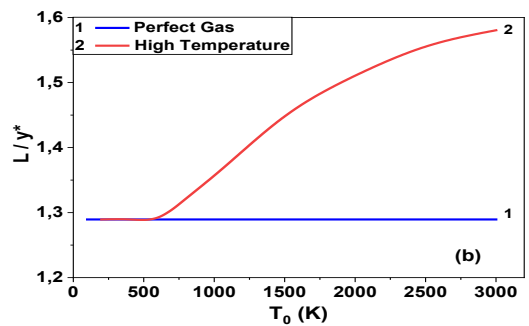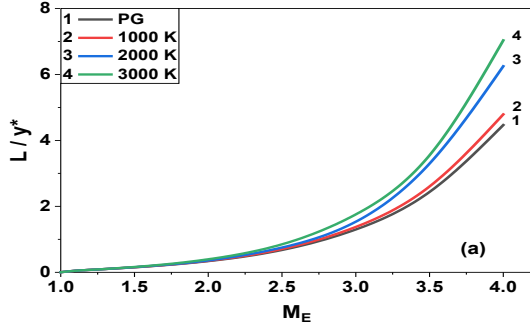

Fig. 19 – Variation of the length of the axisymmetric plug nozzle. (a) Versus the exit Mach number M_E. (b) Versus the temperature T_0

Figure 20 shows the variation of the mass coefficient C_{mass} of the axisymmetric plug nozzle as a function of the exit Mach number M_E for different values of the temperature T_0 and for the perfect gas case.

It should be noted that the difference between the PG curve and the HT curves obtained for the different temperatures T_0 is negligible for an exit Mach number lower than 2.00.

This difference becomes considerable and increases more when the exit Mach number M_E increases.

It is concluded that more the nozzle produces a high exit Mach number, the greater its mass. We also note that the curves corresponding to the PG model and to a temperature $T_0 = 1000\ K$ are almost coincident for all the values of M_E. Thus, it can be concluded that the PG model can be used for T_0 less than $1000\ K$.
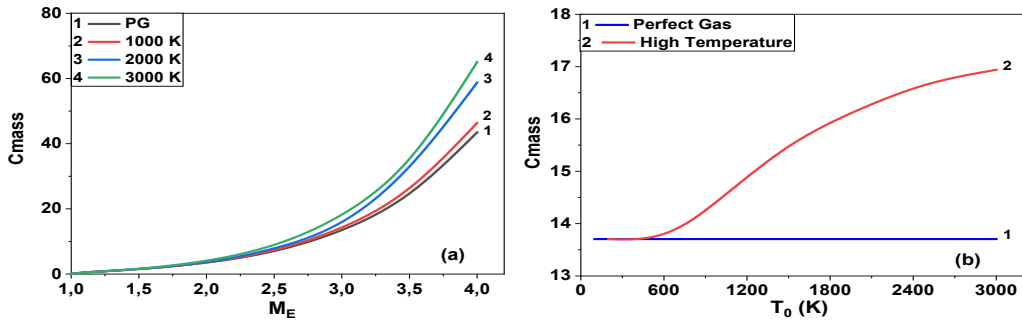
Fig. 20 – Variation of the Mass coefficient C_{mass} of the axisymmetric plug nozzle. (a) Versus the exit Mach number M_E . (b) Versus the temperature T_0

Figure 21 shows the variation of the thrust coefficient exerted on the profile of the nozzle with an axisymmetric plug nozzle as a function of the exit Mach number M_E for different values of the generating temperature T_0 as well as for the case of an ideal gas.

It should be noted that the influence or the effect of the temperature T_0 on the thrust coefficient C_F is negligible when the exit Mach number M_E is less than 1.50; but beyond this value, the difference between the curves of the HT model gradually increases with increasing M_E.
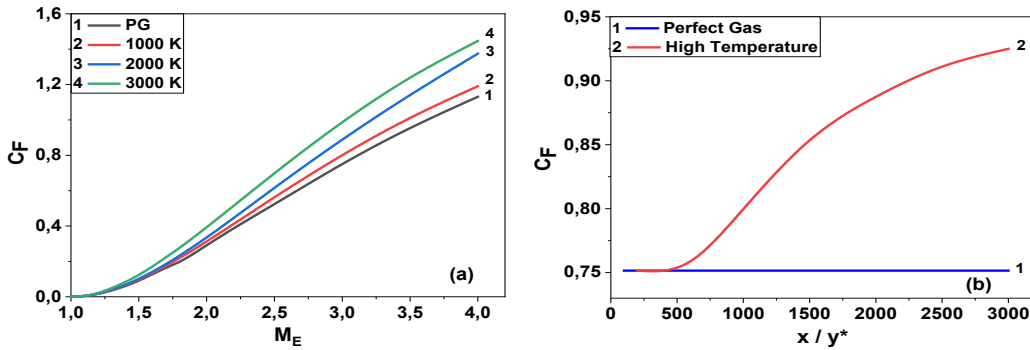

Fig. 21 – Variation of the thrust coefficient C_F of the axisymmetric plug nozzle. (a) Versus the exit Mach number M_E . (b) Versus the temperature T_0

Figure 22 shows the variation of the section ratio ($\frac{A_E}{A^*}$) of the axisymmetric plug nozzle as a function of the exit Mach number M_E for different values of the generating temperature T_0 as well as for the case of a perfect gas.

Note that the evolution of the section ratio ($\frac{A_E}{A^*}$) is identical to that of the length of the nozzle as a function of the exit Mach number M_E for the case of an ideal gas and for the case of the HT model.

It should also be noted that the four curves are almost coincident at low values of exit Mach number; i.e. up to about $M_E = 2.00$; but, from this value of M_E, the differences between the four curves become larger and larger.

It can be concluded that if the exit Mach number M_E is less than 2.00, we can use the PG model instead of using our HT model.
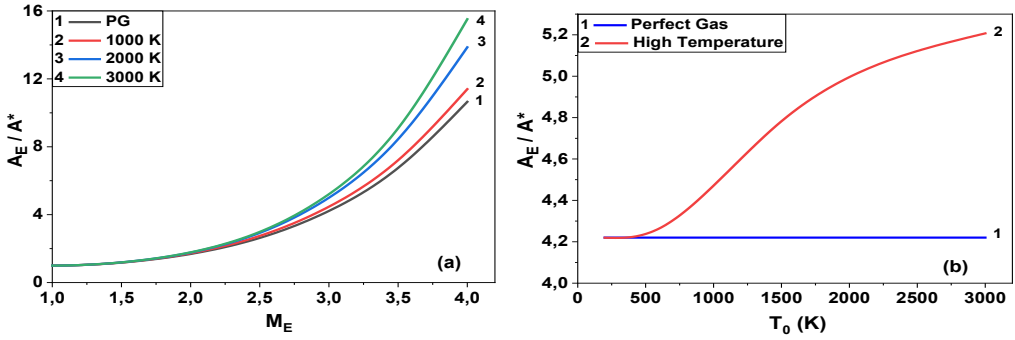
Fig. 22 – Variation of the section ratio $\frac{A_E}{A^*}$ of the axisymmetric plug nozzle. (a) Versus the exit Mach number M_E. (b) Versus the temperature T_0

4.2 The error induced by the Perfect Gas model

The specific heat C_P constant, which yields acceptable results for low T_0 and M_E, is taken into account while developing the perfect model (PG).

In accordance with this investigation, a distinction between the PG model and our HT model outcomes will be shown.

It is possible to determine the error provided by the PG model relative to our HT model for each parameter.

For the length $(\frac{L}{y^*})$, section ratio $(\frac{A_E}{A^*})$, mass coefficient (C_{mass}), and thrust coefficient (C_F), Fig. 23-26 show the evolution of the relative error versus M_E.

A relative inaccuracy of $\varepsilon = 15.315\%$ for length, $\varepsilon = 15.529\%$ for section ratio, $\varepsilon = 15.490\%$ for mass coefficient, and $\varepsilon = 16.147\%$ for thrust coefficient will be produced by the usage of the PG model, for instance, if $T_0 = 2000\ K$ and $M_E = 3.00$.

The adoption of the PG model when $T_0 < 1000\ K$ or $M_E < 2.00$ interprets the error as being weak (less than 5%) for lower values of M_E and T_0.
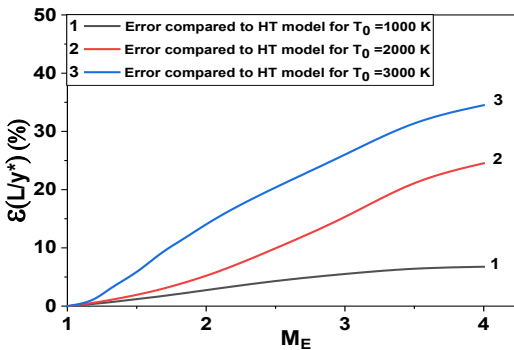

Fig. 23 – Variation of the relative error given by the length of the PG and HT models versus M_E
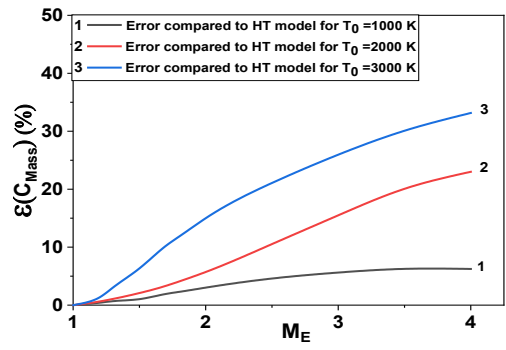
Fig. 24 – Variation of the relative error given by the Mass coefficient of the PG and HT models versus M_E
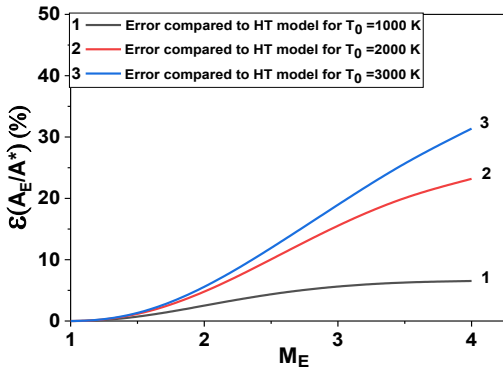
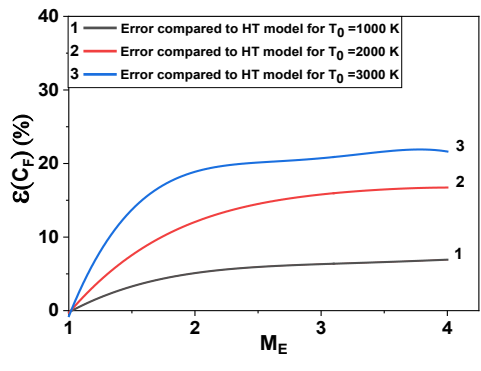Fig. 25 – Variation of the relative error given by the section ratio of the PG and HT models versus M_E

Fig. 26 – Variation of the relative error given by the thrust coefficient of the PG and HT models versus M_E

In plug nozzles, the wall section is substantially constant and therefore it contributes only a few percent to the total thrust. For reasons of optimization, these nozzles must be truncated in order to increase their performance. One of the main advantages of the plug nozzles is that their performance is not dramatically changed if the plug is truncated at even a small fraction of its length. Indeed, the ending part of the plug (like in the case of conventional nozzles) is fairly flat and its contribution to thrust is a small fraction of the overall nozzle thrust, as the force acting on the plug wall is nearly perpendicular to nozzle axis.

Figure 27 shows the coefficient of the mass gain and the loss of thrust coefficient calculated by the computation code from axisymmetric plug nozzle, truncated to any section from the exit section to the throat.
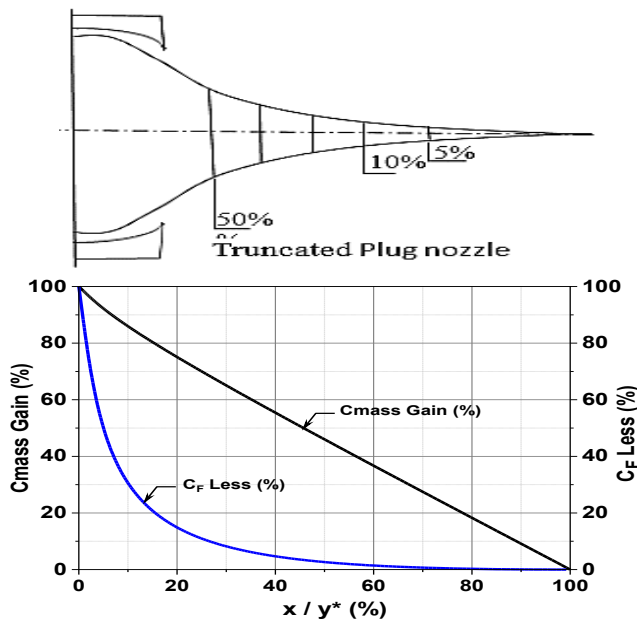

Fig. 27 – Representation of the gain in mass and the C_F loss of a truncated axisymmetric plug nozzle for $M_E = 3.00$ and $T_0 = 2000\ K$

Table 5 summarizes the performance of the truncated nozzles at the cross sections between 0% and 30% with respect to the length of the nozzle ($\frac{L}{y^*}$).

Table 5 – Effect of the stagnation temperature T_0 on the axisymmetric plug nozzle design for $M_E = 5.00$

Trancated Nozzle at	$\dfrac{L}{y^*}$	Gain % (C_{mass})	Less % (C_F)
0%	1.5438	0.0000	0,0000
5%	1.4667	4,4665	0,4715
10%	1.3894	9,1548	0,2210
15%	1.3122	13,740	0,5613
20%	1.2351	18,312	0,3860
25%	1.1579	22,890	0,1937
30%	1.0807	27,487	0,3590

5. CONCLUSIONS

The purpose of this research is to investigate the impact of stagnation temperature on flow characteristics and the design of an axisymmetric plug nozzle at high temperature (HT model). For the first time, a computer code written in FORTRAN program is used for a perfect gas (PG model) and was developed for the high temperature case (HT model). For values of M and T_0 lower than 2.00 and 1000 K respectively, the PG model gave very satisfactory results. As M_E and T_0 increase, this affects performance, requiring the use of our HT model to correct the calculations. This computer code gives results for any gas encountered in nature. The $C_P(T)$ and $\gamma(T)$ values of the gas are combined to use the HT model. By eliminating all of the interpolation constants of the function $C_P(T)$ except the first one, we can obtain the relations of the perfect gas from the relations of the HT model. The PG model thus turns into a special case of our HT model in this situation.

The application was made on the air. It was found that the design and parameters of the axisymmetric plug nozzle are significantly influenced by the functions $C_P(T)$, R, and $\gamma(T)$. But our HT model requires more calculation time for the results to converge than the PG model needs for the same precision. If an inaccuracy of less than 5% is acceptable, a supersonic flow may be studied using the PG relations if the stagnation temperature is less than 1000 K for any value of the Mach number, or when the Mach number is less than 2.00 for any stagnation temperature up to around 3500 K.

For several stagnation temperatures T0, the error between the HT and PG models is calculated for various parameters (length, exit section, thrust coefficient, and mass coefficient). For $T_0 = 2000 K$ and $M_E = 3.00$, the PG model yields relative inaccuracies of $\varepsilon = 15.315\%$ for length, $\varepsilon = 15.529\%$ for section ratio, $\varepsilon = 15.490\%$ for mass coefficient, and $\varepsilon = 16.147\%$ for thrust coefficient.

This error increases in proportion to the temperature. We can create an extension that uses the stream-lines approach in space to calculate the physical characteristics of a plug nozzle design at high temperature of any arbitrary 3D section, such as applications for square or rectangular forms [18].

REFERENCES

[1] K. Herman, F. W. Crimp, Performance of plug-type rocket exhaust nozzles, *ARS Journal,* vol. **31**, no. 1, pp. 18-23, 1961.

[2] G. A. Arnold, *Patent No. 2,683,962*, Washington, DC: U.S. Patent and Trademark Office, 1954.

[3] W. H. Krase, Performance analysis of plug nozzles for turbojet and rocket exhausts, *ASME 1959 Gas Turbine Power Conference and Exhibit, American Society of Mechanical Engineers,* Ohio, USA, 1959.

[4] E. Balasaygun, *Experimental analysis of plug nozzles*, M. S. dissertation, University of Arizona, USA, 1964.

[5] G. Angelino, Approximate method for plug nozzle design, *AIAA J.,* vol. **2**, no. 10, pp. 1834-1835, 1964.

[6] G. V. Rao, Spike nozzle contour for optimum thrust, *Planetary and Space Science,* vol. **4**, pp. 92-101, 1961.

[7] A. Shahrokhi, S. Noori, Survey of the central plug shape of the aerospike nozzle, *17th Australasian Fluid Mechanics Conference*, Auckland, New Zealand, 2010.

[8] V. K. Shanmuganathan, N. Gayathri, S. Kabilan, K. Umanath, Comparative study on performance of linear and annular aero-spike nozzles, *Aust J Basic Appl Sci*, vol. **9**, no. 11, pp. 883-892, 2005.

[9] E. Besnard, H. H. Chen, T. Mueller, J. Garvey, Design, manufacturing and test of a plug nozzle rocket engine, *AIAA Paper 02-4038.*

[10] N. K. Kumar, M. Gopalsamy, C. Antony, R. Krishnaraj, C. B. Viswanadh, Design and optimization of aerospike nozzle using CFD, *IOP Conference Series: Materials Science and Engineering,* Coimbatore, India, 2017.

[11] K. Chutkey, B. Vasudevan, N. Balakrishnan, Analysis of annular plug nozzle flowfield, *Journal of spacecraft and rockets,* vol. **51**, no. 2, pp. 478-490, 2014.

[12] C. H. Wang, Yu Liu, Li-Zi Qin, Aerospike nozzle contour design and its performance validation*, Acta Astronautica,* vol. **64**, no. 12, 1264-1275, 2009.

[13] O. Abada, T. Zebbiche, A. Abdallah Elhirtsi, Three-dimensional supersonic minimum length nozzle design at high temperature for arbitrary exit cross section, *Arabian Journal for Science and Engineering*, vol. **39**, no. 11, pp. 8233-8245, 2014.

[14] G. R. Johnson, H. D. Thompson, J. D. Hoffman, Design of maximum thrust plug nozzles with variable inlet geometry, *Computers & Fluids,* vol. **2**, no. 2, pp. 173-190, 1974.

[15] I. Takashi, K. Fujii, A. K. Hayashi, Computations of axisymmetric plug-nozzle flowfields: Flow structures and thrust performance, *Journal of Propulsion and Power,* vol. **18**, no. 2, pp. 254-260, 2002.

[16] T. Zebbiche, Stagnation temperature effect on the supersonic axisymmetric minimum length nozzle design with application for air, *Advances in space research,* vol. **48**, no. 10, pp. 1656-1675, 2011.

[17] J. H. Ruf, P. K. McConnaughey, A numerical analysis of a three-dimensional aerospike, *AIAA Paper.*

[18] S. B. Verma, Performance characteristics of an annular conical aerospike nozzle with freestream effect, J*ournal of Propulsion and Power,* vol. **25**, no. 3, pp. 783-791, 2009.

[19] G. Hagemann, H. Immich, M. Terhardt, Flow phenomena in advanced rocket nozzles- the plug nozzle, *AIAA Paper.*

[20] Y. H. Liu, Experimental and numerical investigation of circularly lobed nozzle with/without central plug, *International Journal of Heat and Mass Transfer,* vol. **45**, no. 12, pp. 2577-2585, 2002.